Numerical Methods for Two-Fluid Dispersive Fast MHD Phenomena

Bhuvana Srinivasan[1,*], Ammar Hakim[2] and Uri Shumlak[1]

[1] *Aerospace and Energetics Research Program, University of Washington, Seattle, WA 98195, USA.*
[2] *Tech-X Corporation, 5621 Arapahoe Avenue Suite A, Boulder, CO 80303, USA.*

Abstract. The finite volume wave propagation method and the finite element Runge-Kutta discontinuous Galerkin (RKDG) method are studied for applications to balance laws describing plasma fluids. The plasma fluid equations explored are dispersive and not dissipative. The physical dispersion introduced through the source terms leads to the wide variety of plasma waves. The dispersive nature of the plasma fluid equations explored separates the work in this paper from previous publications. The linearized Euler equations with dispersive source terms are used as a model equation system to compare the wave propagation and RKDG methods. The numerical methods are then studied for applications of the full two-fluid plasma equations. The two-fluid equations describe the self-consistent evolution of electron and ion fluids in the presence of electromagnetic fields. It is found that the wave propagation method, when run at a CFL number of 1, is more accurate for equation systems that do not have disparate characteristic speeds. However, if the oscillation frequency is large compared to the frequency of information propagation, source splitting in the wave propagation method may cause phase errors. The Runge-Kutta discontinuous Galerkin method provides more accurate results for problems near steady-state as well as problems with disparate characteristic speeds when using higher spatial orders.

*Corresponding author. *Email addresses:* srinbhu@u.washington.edu (B. Srinivasan), ammar@txcorp.com (A. Hakim), shumlak@u.washington.edu (U. Shumlak)

1 Introduction

There are a number of equation systems that are either hyperbolic or contain hyperbolic parts. Homogeneous, hyperbolic equation systems are written as conservation laws of the form [1, 2]

$$\frac{\partial \mathbf{Q}}{\partial t} + \nabla \cdot \mathbf{F} = 0, \tag{1.1}$$

where $\mathbf{Q} \in \mathbb{R}^m$ represents the m conserved variables and $\mathbf{F} \in \mathbb{R}^{m \times d}$ represents fluxes in d spatial directions. For all unit vectors $\omega \in \mathbb{R}^d$ the flux Jacobian, $\partial(\mathbf{F} \cdot \omega)/\partial \mathbf{Q}$, has real eigenvalues and a complete set of right eigenvectors. Some homogeneous, hyperbolic equation systems include the Euler equations and magnetohydrodynamic (MHD) equations.

Inhomogeneous, hyperbolic equation systems are described by balance laws of the form

$$\frac{\partial \mathbf{Q}}{\partial t} + \nabla \cdot \mathbf{F} = \mathbf{S}, \tag{1.2}$$

where $\mathbf{S} \in \mathbb{R}^m$ represents the source terms. The source Jacobian for Eq. (1.2) is $\partial \mathbf{S}/\partial \mathbf{Q}$. The presence of real eigenvalues in the source Jacobian results in an equation system that contains diffusive sources. The Navier-Stokes equations and the 10-moment fluid equations [3] are examples of inhomogeneous, hyperbolic equation systems containing diffusive source terms.

For inhomogeneous, hyperbolic equation systems described by Eq. (1.2), the presence of imaginary eigenvalues in the source Jacobian results in an equation system that contains dispersive sources. The two-fluid plasma model is a system of inhomogeneous, hyperbolic equations containing dispersive source terms. The dispersive source terms arise from the physical properties of the plasma medium. Dispersive source terms present a unique challenge for numerical algorithms because low-order, explicit-time-stepping schemes can be unstable when applied to the wave equation leading to numerical dispersion [4]. The physical dispersion can be difficult for numerical schemes to capture and can be difficult to distinguish from the numerical dispersion or "noise". In this paper, numerical methods for solving inhomogeneous, hyperbolic equations containing dispersive source terms are investigated for accuracy and computational effort.

Hyperbolic conservation laws can have discontinuous solutions even if the initial conditions are smooth, and this makes the approximation of the solution difficult. First order upwind methods are needed to effectively capture such discontinuities. However, first order methods are highly diffusive in smooth regions. Second order extensions can be constructed which both resolve the discontinuities and provide better accuracy in smooth regions. Smooth nonlinear solutions can achieve second order accuracy when using Godunov's method with second order corrections [5] even though the method is formally first order accurate, e.g., in Section 15.6 of [2]. [5] provides proof of second order accuracy for smooth problems including the case with source terms (Section 7 of [5]). For

a certain class of finite volume methods such as the high-resolution wave propagation method, the solution can be diffusive when eigenvalues of the flux Jacobian have a significant spread. Higher than second order extensions are thus needed. In this paper a higher-order ($> \mathcal{O}(1)$) finite volume method [2,5] and a spectrally accurate finite element method [6] are applied to the plasma fluid equations.

The wave propagation method belongs to the class of finite volume methods. The domain is discretized into cells and the cell averages of the conserved variables are evolved. A Riemann problem is solved at each cell edge and is used to compute the numerical fluxes. Using these computed fluxes, the solution is then updated in the cells connected to that edge. To achieve higher than first order accuracy a linear reconstruction of the waves is performed at the edge which allows up to a second order accurate solution. Limiters are applied to reduce the spatial order in the regions of large gradients whereas regions of small gradients maintain higher-order. For simulations with strong shocks, limiters often reduce the solution to first order around the shocks.

The Runge-Kutta discontinuous Galerkin (RKDG) method is a finite element method. While the wave propagation method is second order, the discontinuous Galerkin method achieves higher spatial order accuracy by expanding the solution in basis functions defined locally in each cell. The order of the polynomial determines the spatial order of the method. As in the case of the wave propagation method, Riemann problems are solved at the cell edge. The data for the Riemann problem are computed using the basis function expansion. A Runge-Kutta time stepping method is used to advance the solution in time.

An overview of the development of discontinuous Galerkin (DG) methods is provided by Cockburn, Karniadakis and Shu in [7]. DG methods were originally developed in the framework of neutron transport equations by Reed and Hill [8] for solving linear hyperbolic equations. The DG method was then applied to non-linear advection-dominated hyperbolic systems by Cockburn and Shu [9] who used the high-order TVD Runge-Kutta time integration that was developed by Shu [10] with DG and developed local projection slope-limiters to balance the spurious oscillations in regions of sharp gradients. This was extended to higher spatial orders and multiple dimensions for applications to non-linear systems such as the Euler equations.

Next came the evolution of the DG method for applications to advection-diffusion equation systems [6, 11, 12], such as the Navier-Stokes equations. The DG method has also been applied to Maxwell's equations [13, 14] where the electromagnetic oscillations need to be appropriately resolved and to single-fluid MHD equations [15] where the plasma waves need to be appropriately resolved. The application of DG methods to nonlinear dispersive equations, specifically the Korteweg-de Vries equation, is explored in [16] where DG methods are shown to be advantageous in the presence of rapid oscillations and are capable of simultaneously capturing oscillations and discontinuous fronts in the solution. Zhang and Shu have compared the discontinuous Galerkin method to spectral finite volume methods in [17] for linear one-dimensional hyperbolic equations and state that the spectral finite volume method has larger errors than the DG method on the same mesh.

The plasma fluid equations studied in this paper differ from previously published work because the dispersive nature of the non-linear balance laws originates from the purely dispersive source terms. The appropriate treatment of advection and dispersion terms and the complications that arise from the presence of significant dispersion in plasma models provide a unique set of comparisons between the wave propagation and the RKDG methods. There is very little literature regarding the numerical solution of hyperbolic equation systems that contain dispersive source terms without the presence of any explicit dissipation [4, 18]. Hakim, Loverich and Shumlak [4] implement the high-resolution wave propagation method for the two-fluid plasma model studied in this paper. Loverich and Shumlak [18] implement the Runge-Kutta discontinuous Galerkin method for the two-fluid plasma model. Neither of these references address the effect of the physical dispersive source terms of the two-fluid plasma model on the accuracy of the numerical methods.

The two-fluid equations describe the self-consistent evolution of electron and ion fluids in the presence of electromagnetic fields. The two-fluid plasma equation system is different from Euler equations or Navier-Stokes equations that have been previously studied with the discontinuous Galerkin method. The two-fluid plasma equations are dispersive and not dissipative. The dispersion is not a numerical artifact. The dispersive nature is a physical effect that leads to the wide variety of plasma waves. The plasma waves in this paper are fast MHD waves that result from resolving the ion and electron plasma frequencies in the presence of electromagnetic waves. Mathematically, the dispersive effects are generated from the source terms of the two-fluid plasma equations described in Section 2.2. The dispersive nature of these equation systems sets them apart from previous publications. The study of the appropriateness of the wave propagation and the discontinuous Galerkin methods to accurately capture these physical dispersive effects is a main point of the manuscript.

Section 2 describes the full two-fluid plasma model showing the basic equations and performing a source term analysis to highlight the physically expected dispersion brought about by the sources. Section 3 briefly describes the high-resolution wave propagation method and Section 4 briefly describes the RKDG method. Section 5 presents a convergence study using a linear advection equation to quantify the spatial order for the RKDG and wave propagation methods. Section 6 explores a benchmark problem that uses the wave propagation method and the RKDG method. The benchmark problem uses the Euler equations with the addition of dispersive source terms. This provides a model equation system for the two-fluid plasma model. Following a study of the wave propagation and RKDG methods for the benchmark problem, the numerical methods are applied to the two-fluid plasma problems in Section 7.

The simulations are performed using the WARPX (Washington Approximate Riemann Plasma) code developed at the University of Washington. WARPX is written in C++ and provides a general framework for developing parallel computational physics algorithms. The wave propagation and the RKDG methods are implemented for arbitrary hyperbolic conservation laws and use the same underlying approximate Riemann solvers

and flux calculation methods wherever appropriate. This allows a fair comparison of the methods since they both use the same optimized framework to solve the equations. All simulations presented in this paper are performed on rectangular, regular meshes.

2   Full two-fluid plasma model

The full two-fluid plasma model [19] used in this section is derived by taking moments of the Boltzmann equation and treating the electrons and ions as two separate fluids. The resulting Euler equations are used to evolve the electron and ion fluids while Maxwell's equations are used to evolve the electromagnetic terms. The equations that result have homogeneous, hyperbolic parts and inhomogeneous source terms.

2.1   Governing equations for the full, two-fluid plasma model

The equations described here are the five-moment equations that result from taking the zeroth, first and second moments of the Boltzmann equation. These moment equations are closed with an equation of state. Assumptions used are isotropic pressure, no heat flux and no frictional forces. The electrons and ions are each described by the Euler equations with source terms coupling the fluids and the fields. In balance law form, the fluid equations are

$$\frac{\partial \rho_s}{\partial t} + \nabla \cdot (\rho_s \mathbf{u}_s) = 0, \tag{2.1a}$$

$$\frac{\partial \rho_s \mathbf{u}_s}{\partial t} + \nabla \cdot (\rho_s \mathbf{u}_s \mathbf{u}_s + p_s \mathbf{I}) = \frac{\rho_s q_s}{m_s} (\mathbf{E} + \mathbf{u}_s \times \mathbf{B}), \tag{2.1b}$$

$$\frac{\partial \epsilon_s}{\partial t} + \nabla \cdot \left((\epsilon_s + p_s) \mathbf{u}_s \right) = \frac{\rho_s q_s}{m_s} \mathbf{u}_s \cdot \mathbf{E}, \tag{2.1c}$$

where subscript, s, denotes electron or ion species. q_s is the species charge, m_s is the species mass, ρ is the mass density, $\mathbf{u}$ is the velocity, $\mathbf{E}$ is the electric field, $\mathbf{B}$ is the magnetic field, p is the pressure and ϵ is the total energy. The energy is defined as

$$\epsilon_s \equiv \frac{p_s}{\gamma - 1} + \frac{1}{2} \rho_s u_s^2. \tag{2.2}$$

Maxwell's equations are used to evolve the electric and magnetic fields.

$$\frac{\partial \mathbf{B}}{\partial t} + \nabla \times \mathbf{E} = 0, \tag{2.3a}$$

$$\frac{1}{c^2} \frac{\partial \mathbf{E}}{\partial t} - \nabla \times \mathbf{B} = -\mu_0 \mathbf{J}, \tag{2.3b}$$

$$\nabla \cdot \mathbf{E} = \frac{\varrho_c}{\varepsilon_0}, \tag{2.3c}$$

$$\nabla \cdot \mathbf{B} = 0, \tag{2.3d}$$

where ϱ_c and **J** are the charge density and the current density defined by

$$\varrho_c \equiv \sum_s \frac{q_s}{m_s}\rho_s, \tag{2.4a}$$

$$\mathbf{J} \equiv \sum_s \frac{q_s}{m_s}\rho_s\mathbf{u}_s. \tag{2.4b}$$

The source terms of Eq. (2.1b) contain the Lorentz forces on the electrons and ions. These source terms couple the fluid equations to the electromagnetic fields. The Lorentz forces act as body forces on the electrons and ions. The evolving electromagnetic source terms can make the equation set and the solutions rather complicated. The full two-fluid equations are applied to the one- and two-dimensional Z-pinch equilibrium. Applications and results of the two-fluid plasma model are presented in Sections 7.3, 7.4, and 7.5.

2.2 Source terms of the two-fluid plasma model

The two-fluid plasma model has physical dispersion that comes about from the presence of dispersive source terms. The source Jacobian for Eq. (1.2) is $\mathbf{J_S} = \partial\mathbf{S}/\partial\mathbf{Q}$. The first three eigenvalues of the source Jacobian are $0, \pm i\omega_p$, where $\omega_p^2 = \omega_{pe}^2 + \omega_{pi}^2$. The plasma frequency is defined as

$$\omega_{ps} = \sqrt{\frac{n_s q_s^2}{\varepsilon_0 m_s}}, \tag{2.5}$$

where subscript s represents each species (electrons and ions). The remaining six eigenvalues are roots of the polynomial with respect to λ,

$$\frac{1}{M^2}\lambda\left(\lambda^2 + \omega_{pe}^2 + \omega_{pi}^2\right)\left[B^4\lambda^2 r_i^4 + M^2\lambda^2(\lambda^2 + \omega_{pe}^2 + \omega_{pi}^2)^2 + B^2 r_i^2\left(M^2\lambda^4\right.\right.$$
$$\left.\left. + \lambda^4 + 2M^2\omega_{pe}^2\lambda^2 + M^2\omega_{pe}^4 + \omega_{pi}^4 + 2(\lambda^2 - M\omega_{pe}^2)\omega_{pi}^2\right)\right] = 0, \tag{2.6}$$

where M is the electron-to-ion mass ratio, r_i is the ion charge-to-mass ratio, and B is the magnitude of the magnetic field. All non-zero eigenvalues, λ, are imaginary.

Since the source Jacobian has only imaginary eigenvalues, the waves of the two-fluid model are not damped. This plasma model is not diffusive but instead is dispersive with undamped oscillations similar to the model equation system using Euler equations with dispersive source terms explored in Section 6. This dispersive nature of the two-fluid plasma model sets the work in this paper apart from previous publications. The wave propagation and RKDG methods are studied for their abilities to capture these physical dispersions accurately. Explicit methods are often unstable when such oscillations are present because refining the grid can excite waves of smaller wavelengths making it difficult to capture the dispersions accurately. The regime of applicability of the wave propagation and RKDG methods is explored in the presence of such dispersions.

3 High resolution wave propagation method

The high resolution wave propagation method can be applied to balance laws of the form Eq. (1.2). This method is described in detail for two-fluid plasma equations in [4]. The wave propagation method belongs to the class of *Godunov methods* which rely on the solution of Riemann problems. The essential idea is as follows. The domain is discretized into cells and the solution in each cell is assumed to be represented by averages. At each cell interface the solution is reconstructed and will, in general, be discontinuous. This discontinuity is used as an initial condition for a Riemann problem. The solution of the Riemann problem gives the conserved variables at the interface which are then used to compute numerical fluxes. Once the fluxes are known the solution in each cell is updated by tallying how much flux flows into the cell.

In one dimension, up to second order accuracy can be achieved by performing a linear reconstruction of the waves needed to compute the numerical fluxes at the cell interface. In multiple dimensions high resolution *transverse corrections* are included which account for flow that is transverse to the coordinate axes. After solving the Riemann problem at each cell interface to determine the positive- and negative-going fluctuations, a second transverse Riemann problem is solved to compute the transverse fluctuations as detailed in [2]. With these transverse corrections, the method is formally second order accurate and is stable to CFL number of unity even when using Godunov splitting, as described in Section 17.5 of [2]. The wave propagation update formula in 1-dimension is given by

$$\mathbf{Q}_i^{n+1} = \mathbf{Q}_i^n - \frac{\Delta t}{\Delta x} \left[\mathcal{A}^+ \Delta \mathbf{Q}_{i-\frac{1}{2}} + \mathcal{A}^- \Delta \mathbf{Q}_{i+\frac{1}{2}} \right] - \frac{\Delta t}{\Delta x} \left([\tilde{\mathbf{F}}]_{i+\frac{1}{2}} - [\tilde{\mathbf{F}}]_{i-\frac{1}{2}} \right), \qquad (3.1)$$

where $\mathcal{A}^+ \Delta \mathbf{Q}_{i-1/2}$ and $\mathcal{A}^- \Delta \mathbf{Q}_{i+1/2}$ are the positive- and negative-going fluctuations, and $[\tilde{\mathbf{F}}]$, is the *correction flux* described in [2].

The source terms for the wave propagation method are handled using source splitting. A Godunov splitting is used here as detailed in [2] where the homogeneous hyperbolic equation is solved first to update the conserved quantities, followed by a Runge-Kutta update to advance the solution with the source terms.

The source terms of the two-fluid system are particularly challenging as they represent undamped oscillations, i.e., the Jacobian of the source terms has purely imaginary eigenvalues. Such sources add physical dispersion to the system which can be difficult to resolve. For a discussion relevant to the two-fluid system, see [4].

4 Discontinuous Galerkin method

The RKDG method is a finite element method. The RKDG method achieves higher spatial order by expanding the solution in polynomial basis functions. The balance law described in Eq. (1.2) is multiplied by a set of basis functions and is integrated over the element. The conserved variable is defined as a linear combination of the basis functions.

In this paper tensor products of the Legendre polynomials are chosen as basis functions. This allows the construction of methods of arbitrary spatial order. Riemann problems are solved at each interface to compute the interface fluxes needed in the algorithm. In general, simple approximate solvers can be used with the RKDG method when using high spatial orders since local fluctuations are accurately represented by the high-order basis-functions [6]. In contrast, the wave propagation method needs a more accurate Riemann solver to avoid diffusive errors. The RKDG method update formula in 1-dimension is given by

$$\frac{d\mathbf{Q}_r}{dt} = -\frac{\mathbf{F}_{i+\frac{1}{2}}v_r\left(x_{i+\frac{1}{2}}\right) - \mathbf{F}_{i-\frac{1}{2}}v_r\left(x_{i-\frac{1}{2}}\right)}{\Delta x} + \frac{1}{\Delta x}\int_{I_i}\frac{dv_r(x)}{dx}\mathbf{F}dx + \frac{1}{\Delta x}\int_{I_i}v_r(x)\mathbf{S}dx, \qquad (4.1)$$

where $\mathbf{Q}_r$ represents the expansion coefficients and v_r represents the polynomial basis functions described in [6].

A 3rd order total variation diminishing (TVD) Runge-Kutta method is used for the time integration as discussed in [6]. This makes the RKDG method an explicit finite element method. When the temporal order is greater than the spatial order, r, the time step is restricted for numerical stability using CFL$\leq 1/(2r-1)$. When the temporal order is smaller than r, the CFL number depends on the accuracy of the Runge-Kutta method [6] and can be more restrictive. Strong stability preserving Runge-Kutta (SSPRK) methods have been explored in recent years and optimal high-order SSP methods have been shown to provide higher temporal accuracy for linear and nonlinear problems with the ability to use larger time steps [20, 21]. While higher-order SSP time integration schemes could be easily extended for use with the DG method used in this paper, there is no benefit gained by using the higher temporal accuracy for the plasma problems explored here because of the relatively smooth temporal evolution. This is verified by exploring the two-fluid model with the 2-dimensional axisymmetric Z-pinch in Section 7.5 using high-order SSPRK methods to show no qualitative differences from the 3rd order TVD RK scheme or even the 2nd order TVB RK scheme. A 3rd order TVD Runge-Kutta method is well suited for time integration for the problems explored in this paper in terms of both accuracy and computational effort.

An *effective resolution* is introduced to provide a fair comparison metric among the numerical methods. The effective resolution takes into account the number of degrees of freedom, i.e., the number of equations being solved for a given spatial order. The wave propagation method solves m equations in N_g cells, where m refers to the number of conserved variables in a given equation system. The degrees of freedom for the wave propagation method is therefore N_g for each variable. The RKDG method solves mr^d equations in N_g cells, where d is the number of dimensions. The RKDG method has $N_g r$ degrees of freedom for each variable, m, in each dimension, d. Therefore, for the RKDG method, the *effective resolution* is defined as $N_g r$.

The RKDG method can produce large oscillations in the solution when sharp gradients are present. As in the case of the wave propagation method, limiters are applied. For the wave propagation method the limiters are applied to the waves, however, for the

RKDG method limiters are applied directly to the conserved variables or the characteristic variables. A modified minmod limiter is used here where the linear terms are checked for oscillations and the high order terms are set to zero if the linear terms need to be limited [22]. Developing high-order limiters is a challenging research problem for the DG method. Some prospective high-order limiters are explored in [23, 24].

5 Convergence study

The linear advection of a one-dimensional Gaussian pulse $q(x,0)=e^{-10(x-1.5)^2}$ is used to numerically determine the spatial order for the wave propagation and RKDG methods. This benchmark problem does not contain any source terms and is included to demonstrate the order of accuracy and convergence for the wave propagation and RKDG methods. The linear advection equation is

$$\frac{\partial q}{\partial t}+\frac{\partial q}{\partial x}=0. \tag{5.1}$$

Periodic boundary conditions on a domain $1 < x < 5$ are used. After propagating the pulse one period through the domain, the l_2 norm of the error is computed by comparing to the exact solution. The spatial order of the method is computed by measuring the dependence of the l_2-norm on the grid spacing.

Table 1: Slopes of l_2-norm vs Δx to determine the order of accuracy of the methods for the linear advection equation. Column 2 shows that the observed spatial order for this problem exceeds the formal order of the methods when using a fixed time-step for all spatial orders. However, column 3 shows the actual order obtained when using the variable time-step with the maximum allowable CFL number (based on the spatial and temporal accuracy of the scheme). The observed temporal order for the higher order RKDG methods is limited by the third-order, time-integration method used for all RKDG solutions.

Method	Order (fixed Δt)	Order (maximum Δt)	CFL (maximum Δt)
WAVE	1.9	1.9	1.0
RKDG 2nd order	2.7	2.0	0.33
RKDG 3rd order	3.4	3.2	0.21
RKDG 4th order	4.2	3.0	0.13
RKDG 8th order	8.0	3.1	0.04

Fig. 1 shows the measured l_2-norms of the solutions obtained for different grid resolutions with a fixed time step that is stable for all the numerical methods tested ($\Delta t=0.0003$). The slopes measured from the linear regions of the plot are listed in the second column of Table 1. The 8th order RKDG solution converges to the analytical solution rapidly so the linear behavior is only observed at lower resolutions. The table shows that the computed order of convergence exceeds the formal order of the methods for this linear problem with a fixed Δt. The fixed time step isolates the effect of the spatial order. Fig. 2 shows the l_2-norms of the solutions obtained for different grid resolutions with a variable time step
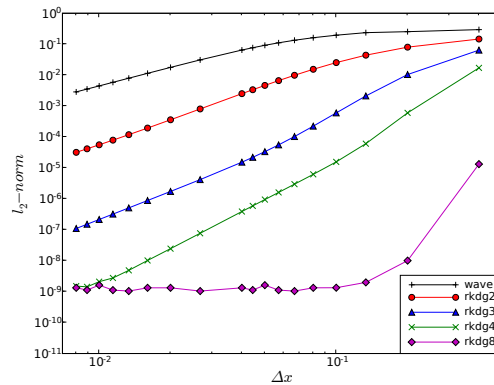
Figure 1: Log-log plot of l_2-norms of solution as a function of Δx for the linear advection problem using a fixed time step to isolate the effect of the spatial order for all the numerical methods - wave propagation, 2nd, 3rd, 4th, and 8th order RKDG. The slopes of the lines are tabulated in Table 1.
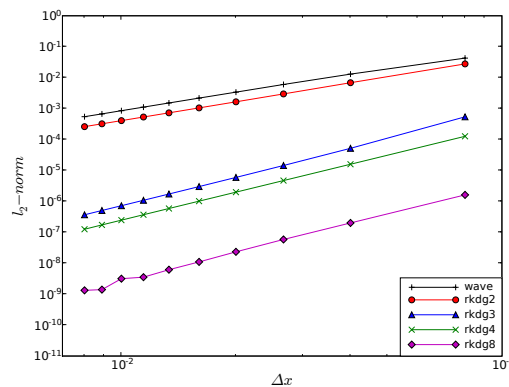

Figure 2: Log-log plot of l_2-norms of solution as a function of Δx for the linear advection problem using the maximum allowable CFL number to set the time step for each of the numerical methods - the wave propagation, 2nd, 3rd, 4th, and 8th order RKDG. The slopes of the lines are tabulated in Table 1.

that is chosen based on the maximum allowable CFL number for each method at each resolution. The maximum CFL number for each method is shown in the 4th column on Table 1 based on the spatial and temporal orders [6]. The slopes measured from the linear regions of the plot are listed in the third column of Table 1. For variable Δt, the computed order of convergence for the higher-order RKDG methods is limited to approximately 3 due to the third-order time-integration method used with the RKDG method.

6   Euler equations with dispersive source terms

Due to the complexity of the full two-fluid plasma system it is difficult to investigate the effects of dispersion on the full non-linear physics. In this section a simpler model is introduced that allows for dispersion to be included with the Euler equations in the form

of dispersive source terms. This provides a model equation system for the two-fluid plasma equations because it generates physical dispersions but has simpler source terms and a closed-form analytical solution exists for the linear case. This equation system models the quasineutral ion cyclotron waves, which are dispersive waves, in a uniform plasma with a magnetic field that is constant in space and time. The momentum equation includes the force from a uniform transverse magnetic field, which produces dispersive effects. The momentum equation (2.1b), simplifies to

$$\rho\left(\frac{\partial \mathbf{u}}{\partial t}+u\frac{\partial}{\partial x}\mathbf{u}\right)+\frac{\partial p}{\partial x}=nq\mathbf{u}\times\mathbf{B}=\rho\omega_c\mathbf{u}\times\hat{\mathbf{b}}, \tag{6.1}$$

where $\rho=m_in$ is the ion mass density, $\mathbf{u}=(u,v)$ is the fluid velocity, p is the pressure, $\mathbf{B}$ is a uniform magnetic field, $\hat{\mathbf{b}}$ is the unit vector of $\mathbf{B}$ and $\omega_c=qB/m_i$ is the cyclotron frequency. The Euler equations of gas dynamics with dispersive source terms are written in one dimensional non-conservative form as

$$\frac{\partial}{\partial t}\begin{pmatrix}\rho\\u\\v\\p\end{pmatrix}+\begin{pmatrix}u&\rho&0&0\\0&u&0&1/\rho\\0&0&u&0\\0&\gamma p&0&u\end{pmatrix}\frac{\partial}{\partial x}\begin{pmatrix}\rho\\u\\v\\p\end{pmatrix}=\begin{pmatrix}0\\v\omega_c\\-u\omega_c\\0\end{pmatrix}, \tag{6.2}$$

where γ is the adiabatic index. The eigenvalues of the source Jacobian are $0,0,\pm i\omega_c$. These compare well with the purely imaginary eigenvalues of the source Jacobian of the two-fluid plasma model described in Section 2.2, the first three of which are $0,\pm i\omega_p$. The undamped oscillations represented by the presence of the cyclotron frequency in the dispersive Euler equations provide a suitable benchmark model for the undamped oscillations of the two-fluid plasma model. The non-zero imaginary eigenvalues indicates that the system has undamped, non-propagating oscillations which combined with the sound wave leads to dispersive waves

$$\omega_n=\pm(k_n^2c_s^2+\omega_c^2)^{\frac{1}{2}}, \tag{6.3}$$

where $c_s\equiv\sqrt{\gamma p_0/\rho_0}$ is the speed of sound and k_n is the wave number.

To study the ability of the methods to capture the dispersion correctly, a problem in the linear regime is solved. The equations are linearized about a static uniform equilibrium with density ρ_0 and pressure p_0. Assuming a perturbed solution of the form $f=f_0+f_1$, where $f\in\{\rho,u,v,p\}$, and where $f_1(x,t)$ is of the form

$$f_1(x,t)=\sum_{n=1}^{\infty}\hat{f}_ne^{i(k_nx+\omega_nt)}, \tag{6.4}$$

linearized equations are obtained

$$\begin{pmatrix}i\omega_n&ik_n\rho_0&0&0\\0&i\omega_n&-\omega_c&ik_n/\rho_0\\0&\omega_c&i\omega_n&0\\0&ik_n\gamma p_0&0&i\omega_n\end{pmatrix}\begin{pmatrix}\rho_1\\u_1\\v_1\\p_1\end{pmatrix}=\mathbf{0}, \tag{6.5}$$
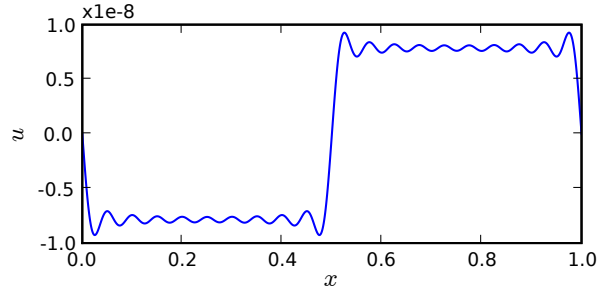
Figure 3: Initial condition with $N=9$ that is used to approximate the step function. This initial condition is used for all the results obtained in this section.

where ρ_1, u_1, v_1, and p_1 depend on n. This system of linear algebraic equations has non-trivial solutions only if ω_n and k_n satisfy the dispersion relation given by Eq. (6.3). The dispersion relation is nonlinear in k_n leading to the dispersion of waves as they propagate through the fluid.

To initialize the simulation the fluid is perturbed with a velocity

$$u_1(x) = u_1^0 \sum_{n=0}^{N} \frac{i}{2n+1} e^{ik_n x} \tag{6.6}$$

with $k_n = 2\pi(2n+1)$ and ω_n computed from Eq. (6.3) and u_1^0 is a constant. As $N \to \infty$, Eq. (6.6) represents a step function for the interval $[0,1]$. With the perturbation of Eq. (6.6), the exact solution for the linearized velocity $u(x,t)$ is given by

$$\tilde{u}(x,t) = - \sum_{n=0}^{N} \frac{u_1^0}{2n+1} \sin(k_n x + \omega_n t). \tag{6.7}$$

The test problem is initialized using the exact solution for all perturbed variables with the velocity given by Eq. (6.7). Fig. 3 shows the initial condition for $u_1^0 = 10^{-8}$, $N=9$ using $\gamma=2$, $\omega_c=10$ and $\rho_0 = p_0 = 1$. For these values the sound speed is given by $c_s = \sqrt{2}$. Periodic boundary conditions are applied on a domain $0 < x < 1$. A CFL number of 1 is used for the wave propagation method and $1/(2r-1)$ is used for the RKDG method. The temporal order of the RKDG method is 3rd order for this problem. Limiters are not applied in either method and the solutions at $t=3$ are compared to the exact solution.

Figs. 4 and 5 compare the analytical solution to the wave propagation method and to the RKDG method. The number of grid elements, N_g, is adjusted with the spatial order, r, of the RKDG method so the effective resolution, $N_g r$, remains constant. Accuracy is measured by taking an l_2-norm. These figures along with Table 2 show that the wave propagation method is more accurate than the 2nd, 3rd and 5th order RKDG methods while all methods have the same effective resolution. The 8th order RKDG solution with only 12 cells, however, is more accurate than the wave propagation method.

The computational time required to advance the solution from $t=0$ to $t=1$ for each method is presented in Table 2. Each method has different CFL stability limit as shown in
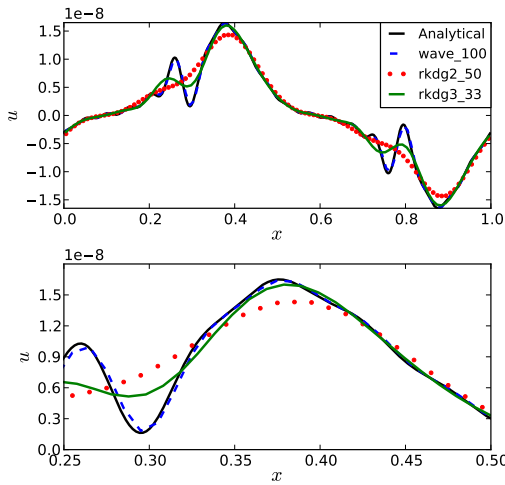
Figure 4: Velocity at $t=3$ for an effective resolution of 100 cells for the wave propagation and RKDG methods, i.e., 100 cells for wave propagation, 50 for 2nd order RKDG and 33 for 3rd order RKDG. $c_s = \sqrt{2}$ and $\omega_c = 10$. The bottom plot has an expanded scale to show the details of the solution.
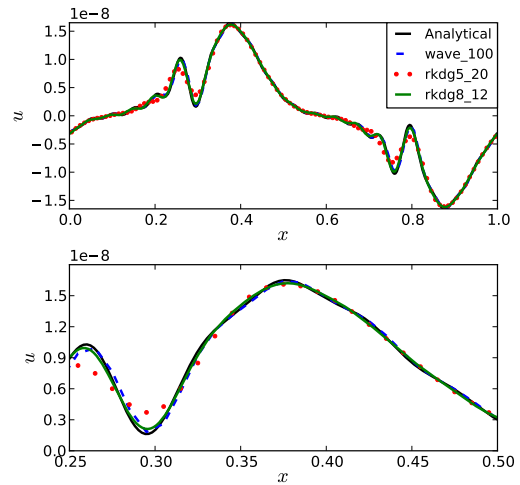
Figure 5: Velocity at $t=3$ with 100 cells for wave propagation, 20 for 5th order RKDG and 12 for 8th order RKDG. $c_s = \sqrt{2}$ and $\omega_c = 10$. The bottom plot has an expanded scale to show the details of the solution.

Table 2: l_2-norm of velocity to quantify accuracy for each method, and computational time required to advance the solution to $t=1$ to quantify computational effort for the dispersive Euler system using $\omega_c = 10$.

Method	l_2-norm	Computational time to $t=1$	CFL
WAVE_100	2.6×10^{-10}	0.02	1.0
RKDG2_50	2.2×10^{-9}	0.03	0.33
RKDG3_33	1.2×10^{-9}	0.04	0.21
RKDG5_20	6.9×10^{-10}	0.07	0.089
RKDG8_12	2.3×10^{-10}	0.19	0.04

the 4th column of Table 2 based on Table 2.2 in [6] where the spatial and temporal orders are taken into account to determine the maximum CFL value. The solution of the wave propagation method is more accurate as compared to the RKDG solutions while using less computational effort for low ω_c. However, when ω_c is increased, the wave propagation method exhibits phase errors in the solution. Fig. 6 shows that the 3rd order RKDG solution using 33 cells is more diffusive than the wave propagation solution at 100 cells, but the RKDG solutions do not have phase errors even at lower orders. Fig. 7 displays results for the wave propagation method with 100 cells, the 8th order RKDG with 12 cells and the 16th order RKDG with 6 cells. Increasing the grid resolution of the wave propagation method from 100 cells to 500 cells reduces the phase error, as shown in Fig. 8, and going to even higher resolution eliminates it.

　　The computational time required to advance the solution from $t=0$ to $t=1$ for each method for $\omega_c = 50$ is presented in Table 3. Table 3 shows that the 16th order RKDG solu-
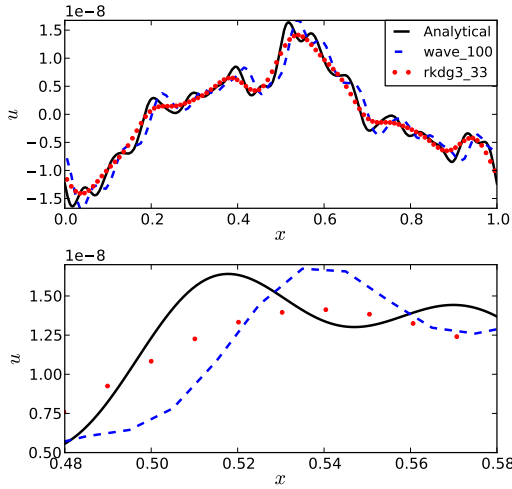
Figure 6: Velocity at $t = 3$ with 100 cells for wave propagation and 33 for 3rd order RKDG. These are for $c_s = \sqrt{2}$ and $\omega_c = 50$. Using a larger ω_c leads to phase errors for the wave propagation method while the lower order RKDG method for the same effective resolution is diffusive but has no phase error. The bottom plot has an expanded scale to show the details of the solution.
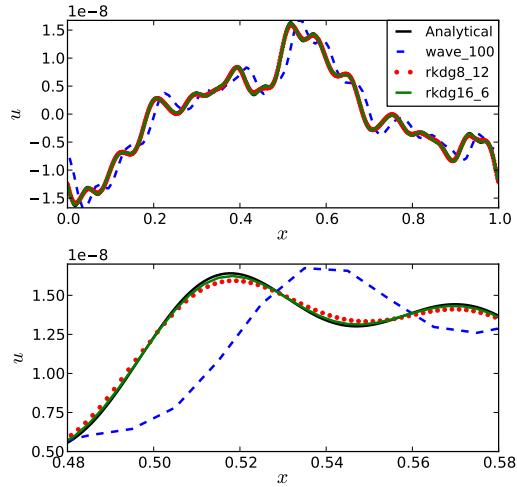

Figure 7: Velocity at $t = 3$ with 100 cells for wave propagation, 12 for 8th order RKDG and 6 for 16th order RKDG. These are for $c_s = \sqrt{2}$ and $\omega_c = 50$. Using a larger ω_c leads to phase errors for the wave propagation method. The bottom plot has an expanded scale to show the details of the solution.
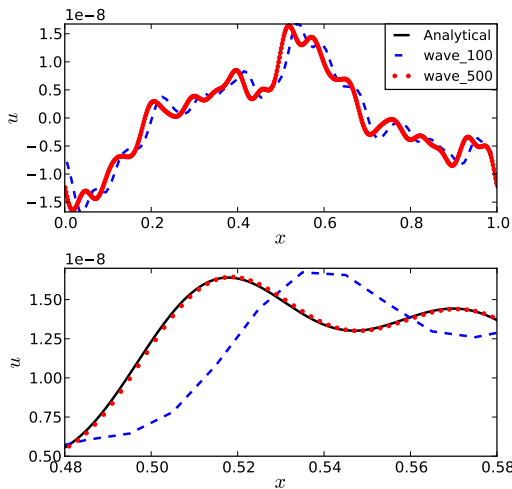

Figure 8: Velocity at $t = 3$ with 100 cells as compared to 500 cells for the wave propagation method. These are for $c_s = \sqrt{2}$ and $\omega_c = 50$. The bottom plot has an expanded scale to highlight the small phase error that is present even with 500 cells when a higher cyclotron frequency is used.
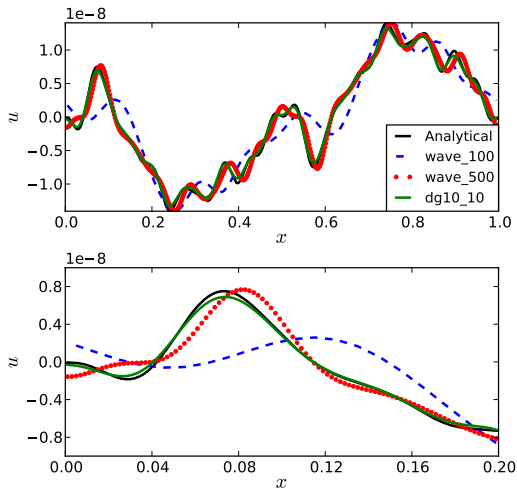

Figure 9: Velocity at $t = 3$ with 100 cells and 500 cells for the wave propagation method as compared to 10 cells for the 10th order RKDG method. These are for $c_s = \sqrt{2}$ and $\omega_c = 100$. The bottom plot has an expanded scale to highlight the phase error that is present even with 500 cells when a higher cyclotron frequency is used.

Table 3: l_2-norm of velocity to quantify accuracy for each method, and computational time required to advance the solution to $t=1$ to quantify computational effort for the dispersive Euler system using $\omega_c=50$.

Method	l_2-norm	Computational time to $t=1$	CFL
WAVE_100	2.2×10^{-9}	0.02	1.0
WAVE_500	1.0×10^{-10}	0.30	1.0
RKDG3_33	1.3×10^{-9}	0.04	0.21
RKDG8_12	2.3×10^{-10}	0.19	0.04
RKDG16_6	6.6×10^{-11}	0.30	0.015

Table 4: l_2-norm of velocity to quantify accuracy for each method, and computational time required to advance the solution to $t=1$ to quantify computational effort for the dispersive Euler system using $\omega_c=100$.

Method	l_2-norm	Computational time to $t=1$	CFL
WAVE_100	2.7×10^{-9}	0.1	1.0
WAVE_500	1.0×10^{-9}	0.4	1.0
RKDG10_10	3.5×10^{-10}	0.18	0.028

tion with only 6 cells is more accurate than the 500 cell wave propagation method. The 16th order RKDG method with only 6 cells uses the same computational effort as the wave propagation method with 500 cells. For large ω_c, the RKDG method provides a more accurate solution even when it is run at a lower effective resolution using high spatial order. For comparable accuracy with large ω_c, the RKDG method uses less computational effort as compared to the wave propagation method. The phase errors in the wave propagation method are caused by the large source terms compared to the advection terms that result from increasing ω_c. This hypothesis is supported by measuring larger phase errors when the source term is increased by setting $\omega_c=100$ as compared to the $\omega_c=50$ solution in Fig. 8. The $\omega_c=100$ results are shown in Fig. 9 and Table 4. In particular, the error for the 500 cell solution is larger for the $\omega_c=100$ solution than for the $\omega_c=50$ solution. When the magnitude of the source term becomes large compared to the advection terms in the equation system, the wave propagation method produces phase errors. Increasing the source term strength for a given resolution increases the error. Table 4 shows that a 10th order RKDG method with 10 cells has higher accuracy and uses less computational effort than a 500 cell wave propagation method when $\omega_c=100$. Hence, the proper handling of source terms becomes critical.

The wave propagation method uses the source term splitting described in Section 3, and this splitting leads to the phase errors. The characteristic oscillation period caused by the source terms is $\tau_c=2\pi/\omega_c$ for the solution. The characteristic time for information to propagate is $\tau_s=\Delta x/c_s$. For the oscillation to be well resolved, τ_c must be sufficiently larger than τ_s. For the case of the wave propagation method with 100 cells, this requirement is violated because $\tau_c=0.126$ while $\tau_s=0.071$, which is not sufficient to resolve τ_s.
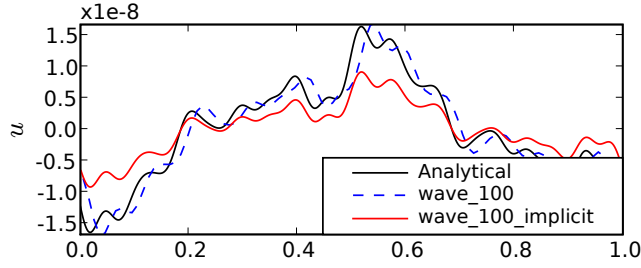
Figure 10: Velocity at $t=3$ with 100 cells for the wave propagation method using source splitting versus using an unsplit implicit source term update. These are for $c_s = \sqrt{2}$ and $\omega_c = 50$. The implicit source update is included to prove that source splitting is responsible for the phase errors. However, the implicit solution is subject to severe diffusion.

The lack of proper sampling leads to the phase error seen in Figs. 7 and 9. The characteristic frequency of the sources introduces ω_c^{-1} time-scales that must be resolved in addition to the other time-scales in the system. The explicit time-step must be sufficiently small for proper sampling of the source frequency such that $\Delta t < \omega_c^{-1}$. To further support that the source splitting causes the phase errors, an unsplit implicit source term update is implemented for the wave propagation method using 100 cells with $\omega_c = 50$. The implicit source term update is described by

$$\mathbf{Q}(t+\Delta t) = \left(\mathbf{I} - \frac{\Delta t}{2}\mathbf{J_S}\right)^{-1}\left[\mathbf{Q}(t) - \Delta t \mathcal{L}(\mathbf{Q}(t)) + \frac{\Delta t}{2}\mathbf{J_S}\mathbf{Q}(t)\right], \tag{6.8}$$

where $\mathcal{L}$ represents the flux update. Fig. 10 shows that while the implicit source term solution is more diffusive, the phase errors are eliminated. Exploring unsplit source term handling for the wave propagation method for equation systems with purely dispersive source terms, without the diffusive nature of an implicit source term update, could make the wave propagation method more robust to such phase error problems.

A von Neumann analysis is performed to specifically quantify the stability condition for the source term update for the wave propagation method. It is noted that as long as the condition

$$\Delta t \leq \frac{2\sqrt{2}}{\omega_c} \tag{6.9}$$

is satisfied, the wave propagation method with a Runge-Kutta source advance is stable in the presence of large ω_c. If a Δt is chosen such that the stability condition in Eq. (6.9) is satisfied, and the time-step accounts for the additional ω_c^{-1} time-scale, the wave propagation solution with 100 cells becomes diffusive. The wave propagation method generally becomes diffusive with CFL numbers less than 1. This presents a numerical difficulty in resolving the physical dispersions accurately while minimizing diffusive errors and requires a higher grid resolution for the wave propagation method. Using higher order spatial representations with the RKDG method solves this problem with less computational effort and greater accuracy in the presence of large source terms.

7   Two-fluid plasma simulations

The two-fluid plasma model described in Section 2 is investigated using the wave propagation and RKDG methods. The two-fluid plasma model contains 18 equations when using the error correction potentials for the purely hyperbolic Maxwell's equations [25]. The error correction potentials provide 2 additional conserved variables to the full two-fluid equation system. They are included as a modification to Maxwell's equations and allow divergence errors to be advected out of the domain at a specified characteristic speed. The challenge with this model lies in resolving all the waves propagating through the domain with speeds ranging from the speed of sound to the speed of light. The error correction speed for the purely hyperbolic Maxwell's equations can be even larger than the speed of light. This section contains four applications of the two-fluid plasma model- a 1-dimensional soliton propagation, an axisymmetric two-fluid pulse in 1-dimension, an axisymmetric Z-pinch equilibrium in 1-dimension and a perturbed axisymmetric Z-pinch equilibrium in 2-dimensions.

7.1   Boundary conditions for axisymmetric problems

Ghost cells are used to specify the boundary conditions for both the wave propagation and the RKDG methods. Using ghost cells allows for the application of Dirichlet boundary conditions where the variables carry a fixed edge value and Neumann boundary condition where the gradient at the boundary is specified.

For axisymmetric problems, the axis boundary condition is implemented at $r = 0$. Appropriate boundary conditions at the axis are found by assuming the variables are analytical about the axis and performing a series expansion about $r = 0$. Radial and azimuthal vector components are set to zero at the axis. Scalar variables and axial vector components have no gradient normal to the axis. To implement the axis boundary condition using ghost cells, the scalar variables and axial vector components are copied into the ghost cells while the radial and azimuthal vector components are copied over to the ghost cells with a negative sign. The problem of singularities at the axis does not arise here because a modal implementation of the DG method is used instead of a nodal implementation.

For problems with conducting wall boundary conditions, the normal velocity, the normal magnetic field, and the tangential electric fields go to 0 at a conducting wall. To implement this boundary condition using ghost cells, all variables are copied from the adjacent domain cells to the ghost cells while reversing the signs of the normal velocity, normal magnetic field and tangential electric fields. The remaining variables are extrapolated from the domain.

The coefficients of the RKDG method must be treated appropriately at the boundaries. As mentioned in Section 4, Legendre polynomials are chosen as the basis functions. The physical boundary conditions are implemented with consideration to the polynomial basis functions of the RKDG method. For example, to implement a Dirichlet boundary

value of zero, the coefficients of all even basis functions in the ghost cells are set to the negative of the adjacent domain cells, and the coefficients of all odd basis functions in the ghost cells are set to the same values as the adjacent domain cells. To make the average value at the boundary zero, the sign is flipped in the ghost cell for all the coefficients of the Legendre polynomial that have even exponents of x since these polynomials are the even basis functions. The polynomials with odd exponents of x are the odd basis functions and do not require a change in sign in the ghost cells. The implementation of the zero gradient at the boundary uses the same procedure with opposite signs for the coefficients of the even and odd basis functions.

7.2 Two-fluid plasma soliton in 1-dimension

The two-fluid plasma model, Eqs. (2.1a)-(2.4b), is applied to one-dimensional soliton propagation [26] where a pulse is initialized in the ion and electron densities and pressures as shown in Fig. 11. The fluid pressures are initialized using fluid temperatures such that $T_i = T_e = 0.01$, and $\mathbf{B}_z = 1$. All other fluid and field variables are initialized to zero. The ion-to-electron mass ratio is 25. The ratio of the speed of light to the electron sound speed, $c/c_{se} = 2$, and the ratio of the speed of light to the ion sound speed, $c/c_{si} = 10$. The speed of light is chosen such that it is the fastest speed in the system. Periodic boundary conditions are used.
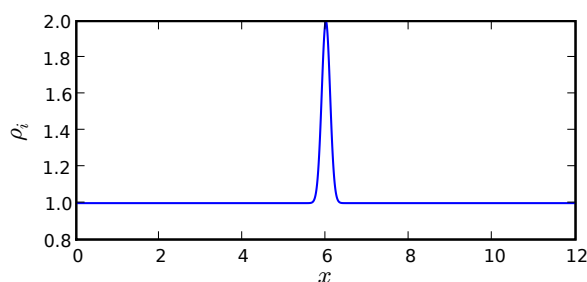

Figure 11: Initial ion mass density for the two-fluid plasma soliton. Ion pressure, electron mass density, and electron pressure have the same profile.

The wave propagation solution at a resolution of 5000 cells is chosen as the converged solution and is used to compare the wave propagation method to the RKDG method. This converged solution is compared to the 3rd order RKDG using 1000 cells to verify that both methods converge to the same solution. Simulations are run to $t = 40$ where time is normalized by the speed of light transit time across the domain. One full period of the ion soliton occurs at $t = 100$. Fig. 12 and Table 5 show that for the same effective resolution of 512 cells, i.e., wave propagation with 512 cells, 2nd order RKDG with 256 cells and 4th order RKDG with 128 cells, the RKDG method provides a more accurate solution than the wave propagation method. Fig. 13 shows that even when the resolution of the wave propagation method is doubled to 1024 cells, the solution is less accurate than the approximate effective resolution of 512 cells using 3rd, 4th, and 5th order RKDG methods.
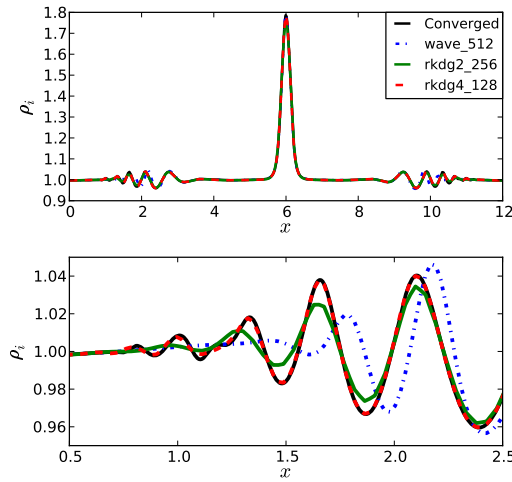
Figure 12: The ion mass density, ρ_i, is compared for the two-fluid plasma soliton using wave propagation and RKDG methods. The solution is shown at $t=40$ with $c=1$. The wave propagation method uses 512 cells, RKDG 2nd order uses 256 cells, and RKDG 4th order uses 128 cells so all methods have the same effective resolution. The bottom plot has an expanded scale to show the details of the solution. The wave propagation method has the largest phase errors.
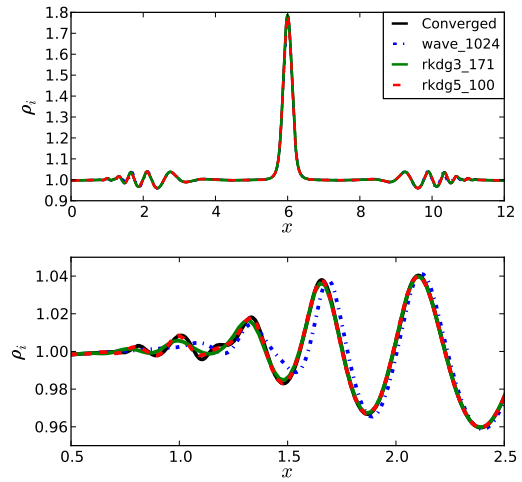
Figure 13: The ion mass density, ρ_i, is compared for the two-fluid plasma soliton using wave propagation and RKDG methods. The solution is shown at $t=40$ with $c=1$. The RKDG 3rd order solution with 171 cells and the RKDG 5th order solution with 100 cells provide a more accurate solution than the 1024 cell wave propagation method at double the effective resolution. The bottom plot has an expanded scale to show the details of the solution.

Phase errors in the wave propagation method solution are evident in the expanded scale plots of Figs. 12 and 13. These phase errors occur in the waves that are propagating away from the initial pulse and result from source splitting just as with the quasineutral ion cyclotron waves explored in Section 6.

Table 5: l_2-norm of ion mass density to quantify accuracy for each method and computational time required to advance the solution to $t=40$ to quantify computational effort for the two-fluid soliton.

Method	l_2-norm	Computational time to $t=40$	CFL
WAVE_512	1.0×10^{-2}	19.6	1.0
WAVE_1024	3.6×10^{-3}	43.2	1.0
RKDG2_256	4.5×10^{-3}	20.8	0.33
RKDG3_171	8.3×10^{-4}	9.96	0.21
RKDG4_128	4.6×10^{-4}	19.5	0.13
RKDG5_100	3.5×10^{-4}	10.3	0.089

The computational time required to advance the solution from $t=0$ to $t=40$ for each method is presented in Table 5. Each method has different CFL stability limit as shown in the 4th column of Table 5 based on Table 2.2 in [6] where the spatial and temporal orders are taken into account to determine the maximum CFL value. When using 1024 cells, the wave propagation method takes 2 times the computational effort as compared to the 4th

order RKDG method using 128 cells, and 4 times the computational effort as compared to the 5th order RKDG method using 100 cells. There does not seem to be an obvious trend in the CPU times for the RKDG method. This nonmonotonic variability in the CPU times is attributed to the stability condition for the RKDG methods described in [6]. CFL$\leq 1/(2r-1)$ is valid for spatial order, r, as long as the temporal order is $r+1$. For all DG spatial orders presented here, a 3rd order Runge-Kutta time integration scheme is used because 2nd order Runge-Kutta time integration is unstable for DG when $r > 2$. In order to use 3rd order Runge-Kutta time integration with $r > 2$, the maximum allowable CFL number is more restrictive as described in [6]. For this problem, the RKDG method provides a more efficient solution when computational effort is taken into account as shown in Table 5. While increasing the grid resolution eliminates the phase errors in the wave propagation method, the RKDG method is more computationally efficient for this problem. Two-dimensional applications of a two-fluid soliton produce similar results.

7.3   Axisymmetric two-fluid plasma pulse in 1-dimension

Following a soliton propagation application, the two-fluid plasma model, Eqs. (2.1a)-(2.4b), is applied to an axisymmetric one-dimensional problem where a pulse is initialized in the axial magnetic field, B_z, as shown in Fig. 14. The electron and ion densities and pressures are initially constant throughout the domain with all other fluid and electromagnetic terms initialized to 0. The ion-to-electron mass ratio is 2.5 to minimize negative pressure errors and allow for faster evolution. The ratio of the speed of light to the electron sound speed, $c/c_{se}=35$, and the ratio of the speed of light to the ion sound speed, $c/c_{si}=55$. Axis boundary conditions are used on the left edge of the domain while conducting wall boundary conditions are used on the right edge. The boundary conditions are treated in the manner described in Section 7.1.
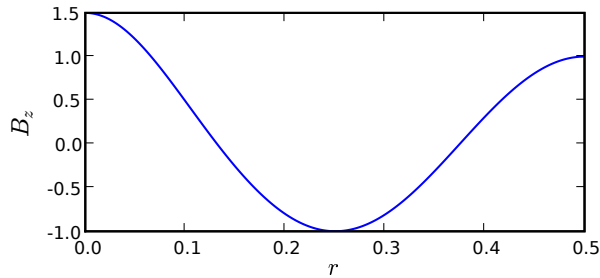

Figure 14: Initial condition for axial magnetic field for the axisymmetric two-fluid plasma pulse.

The wave propagation solution at a resolution of 10,000 cells is chosen as the converged solution and is used to compare the wave propagation method to the RKDG method. This converged solution is compared to the 3rd order RKDG using 1000 cells and it is verified that both methods converge to the same solution. The fluid azimuthal velocity, v_ϕ, shows the largest variation among the methods. For this reason, the electron
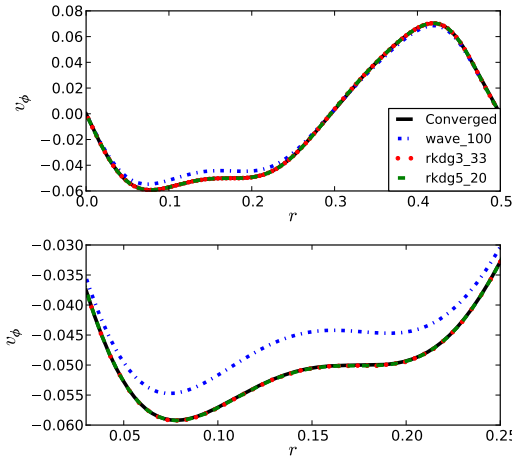
Figure 15: The electron fluid azimuthal velocity, v_ϕ, is compared for the axisymmetric two-fluid plasma pulse using wave propagation and RKDG methods. The solution is shown at $t=0.8$ with $c=1$. The wave propagation method uses 100 cells, RKDG 3rd order uses 33 cells and RKDG 5th order uses 20 cells so all methods have approximately the same effective resolution. The bottom plot has an expanded scale to show the details of the solution. At the same effective resolution, the wave propagation method performs poorest.
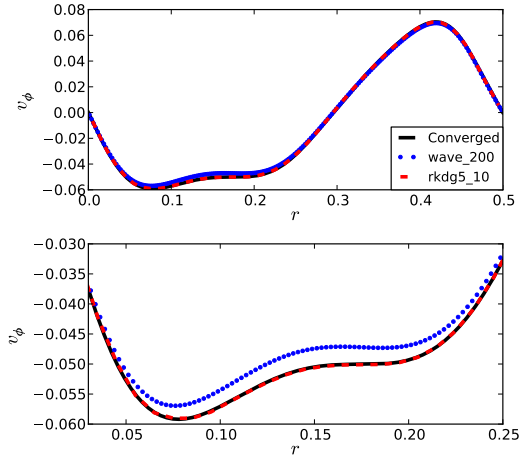
Figure 16: The electron fluid azimuthal velocity, v_ϕ, is compared for the axisymmetric two-fluid plasma pulse using wave propagation and RKDG methods. The solution is shown at $t=0.8$ with $c=1$. The RKDG 5th order solution uses 10 cells with an effective resolution that is 1/4 that of the wave propagation method which uses 200 cells. The bottom plot has an expanded scale to show the details of the solution. Even with a lower effective grid resolution that is 1/4 the resolution of the wave propagation method, the RKDG method provides a more accurate solution than the wave propagation method.

azimuthal velocity is chosen for the comparisons. Simulations are run to $t=0.8$ where time is normalized by the speed of light transit time across the domain. Fig. 15 and Table 6 show that for the same effective resolution of 100 cells, i.e., wave propagation with 100 cells, 3rd order RKDG with 33 cells and 5th order RKDG with 20 cells, the RKDG method provides a more accurate solution than the wave propagation method. Fig. 16 shows that even when the resolution of the wave propagation method is doubled to 200 cells, the solution is less accurate than the effective resolution of 100 cells using 3rd and 5th order RKDG methods. Even the 5th order RKDG method using only 10 cells, i.e., 1/4 the

Table 6: l_2-norm of electron azimuthal velocity to quantify accuracy for each method, and computational time required to advance the solution to $t=0.4$ to quantify computational effort for the two-fluid pulse.

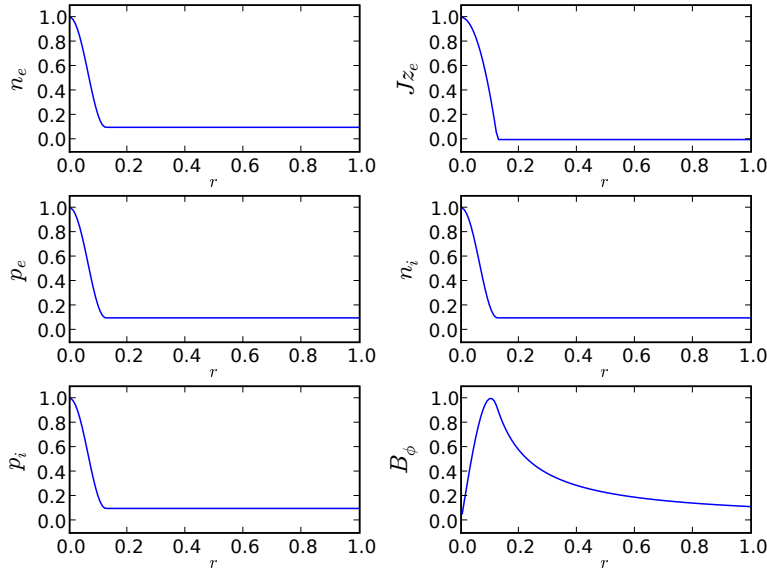| Method	l_2-norm	Computational time to $t=0.4$	CFL
WAVE_100	3.3×10^{-3}	0.04	1.0
WAVE_200	1.7×10^{-3}	0.14	1.0
RKDG3_33	4.2×10^{-5}	0.07	0.21
RKDG5_20	3.6×10^{-5}	0.09	0.089
RKDG5_10	9.9×10^{-5}	0.03	0.089

Figure 17: Initial conditions for the Z-pinch two-fluid equilibrium normalized to the peak values.

effective resolution of the 200 cell wave propagation method, provides a more accurate solution than the wave propagation method with 200 cells as is seen from Table 6. The computational time required to advance the solution from $t=0$ to $t=0.4$ for each method is presented in Table 6. Each method has different CFL stability limit as shown in the 4th column of Table 6 based on Table 2.2 in [6] where the spatial and temporal orders are taken into account to determine the maximum CFL value. When using 200 cells, the wave propagation method takes 2 times the computational effort as compared to the 3rd order RKDG method using 33 cells, and 1.6 times the computational effort as compared to the 5th order RKDG method using 20 cells. The 5th order RKDG method using only 10 cells uses approximately $1/5$ the computational effort of the 200 cell wave propagation method and still provides a more accurate solution.

For this problem, the RKDG method provides a more efficient solution when computational effort is taken into account as shown in Table 6. It is seen that the wave propagation solutions are slightly diffusive for the fluid variables. This can be attributed to the two-fluid plasma model containing disparate wave speeds in the system, namely the fluid speeds of sound and the speed of light. As a result, information propagating at slower characteristic speeds in the system can be diffused. Such diffusion is not seen in the RKDG solutions because the higher spatial and temporal order of the RKDG method provides more accurate solutions even at lower grid resolutions.

7.4 Axisymmetric Z-pinch equilibrium in 1-dimension

The numerical methods are applied to a steady-state problem using the two-fluid plasma model, Eqs. (2.1a)-(2.4b). A one-dimensional, axisymmetric Z-pinch equilibrium is ini-

tialized as shown in Fig. 17.

$$p_0 = \frac{J_0^2}{1-\alpha} \left(\frac{1}{4} R_p^2 - 12 R_p^4 + \frac{4}{3} 128 R_p^6 \right), \tag{7.1a}$$

$$J_{zi} = 0, \tag{7.1b}$$

$$J_{ze} = \begin{cases} J_0 (1 - 64 r^2), & \text{if } r < R_p, \\ 0, & \text{otherwise,} \end{cases} \tag{7.1c}$$

$$B_\phi = \begin{cases} J_0 \left(\frac{1}{2} r - 16 r^3 \right), & \text{if } r < R_p, \\ J_0 \left(\frac{1}{2} R_p - 16 R_p^3 \right) \frac{R_p}{r}, & \text{otherwise,} \end{cases} \tag{7.1d}$$

$$p = \begin{cases} p_0 - J_0^2 \left(\frac{1}{4} r^2 - 12 r^4 + \frac{4}{3} 128 r^6 \right), & \text{if } r < R_p, \\ p_0 - J_0^2 \left(\frac{1}{4} R_p^2 - 12 R_p^4 + \frac{4}{3} 128 R_p^6 \right), & \text{otherwise,} \end{cases} \tag{7.1e}$$

where R_p is the pinch radius, $\rho_i = (m_i/m_e)\rho_e = m_i p / p_0$ and $p_i = p_e = p/2$. In these simulations, $R_p = 1/8$, $\alpha = 1/10$ and $J_0 = 1/10$. The ion-to-electron mass ratio is 25. All remaining variables are initialized to 0. The electron and ion density profiles shift radially a small amount to produce a radial electric field as the initialization adjusts to find an equilibrium.

Axis boundary conditions are used on the left edge of the domain, and conducting wall boundary conditions are used on the right edge.

The wave propagation method is compared to the 2nd, 3rd, 5th and 8th order RKDG methods. The methods are compared for their abilities to maintain equilibrium. The results shown in Fig. 18 are at a characteristic transit time of 20 on a domain $r = 0$ to $r = 1 = 16 r_{Li}$ with a conducting wall on the right boundary. r_{Li} is the ion Larmor radius. The parameters used here are $\gamma = 5/3$, speed of light $c = 1.0$, ion and electron charge-to-mass ratios of $q_i/m_i = 10$, $q_e/m_e = 250$, ion-to-electron mass ratio of $m_i/m_e = 25$, ion Larmor radius-to-domain length of $r_{Li}/x_0 = 1/16$, and ion skin depth-to-domain length of $\delta_i/x_0 = 1/10$. At a characteristic transit time of 20, the 2nd order RKDG and wave propagation solutions are diffusive while the 3rd order RKDG solution maintains equilibrium.

Running the solutions out to a characteristic transit time of 50 gives the results shown in Fig. 19. The higher-order RKDG solutions, i.e., solutions greater than 2nd order, hold equilibrium better than the wave propagation method for the same effective resolution.

When the grid resolution of the wave propagation method is doubled from 128 cells to 256 cells, it requires more computational effort than the 3rd order RKDG method with 40 cells while still being more diffusive than the 3rd order RKDG solution. Investigating this further in Fig. 20 with 5th order RKDG using only 15 cells and 8th order RKDG using only 8 cells it is seen that even at a resolution of 256 cells, the wave propagation method is diffusive as compared to the higher-order RKDG solutions with 1/3 and 1/4 the effective grid resolution. The RKDG method at higher spatial orders holds equilibrium better than the wave propagation method. The 3rd order RKDG solution provides the most accurate solution for the same effective grid resolution as the 128 cell wave propagation
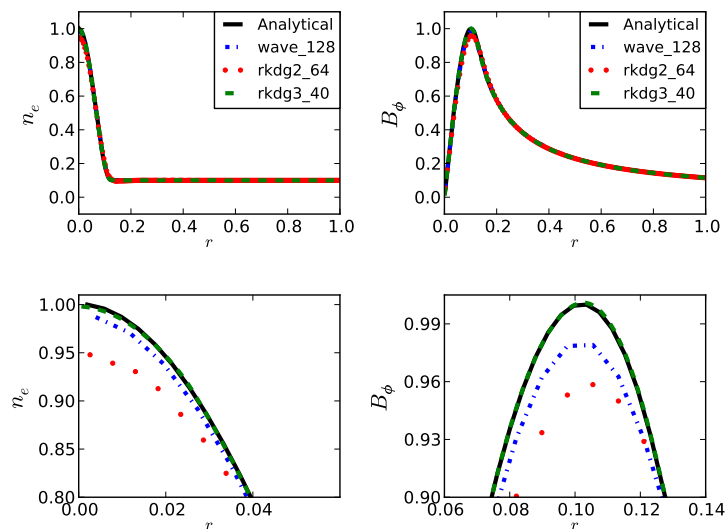
Figure 18: Electron number density and azimuthal magnetic field as functions of radius after 20 characteristic transit times are shown for the two-fluid axisymmetric Z-pinch equilibrium. The wave propagation method uses 128 cells, RKDG 2nd order uses 64 cells and RKDG 3rd order uses 40 cells so all methods have approximately the same effective resolution. The solutions of the wave propagation method and 2nd order RKDG are diffusive. All values normalized to the initial peak values. Lower plots have an expanded scale to show the details of the solution.
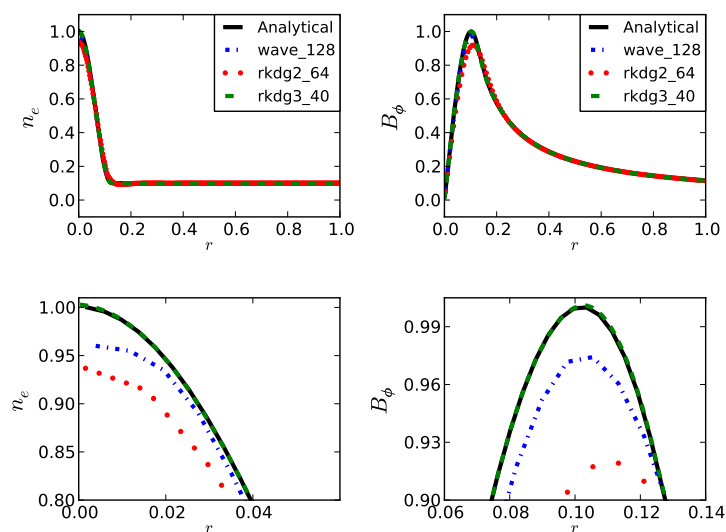

Figure 19: Electron number density and azimuthal magnetic field as functions of radius after 50 characteristic transit times are shown for the two-fluid axisymmetric Z-pinch equilibrium. The wave propagation method uses 128 cells, RKDG 2nd order uses 64 cells and RKDG 3rd order uses 40 cells so all methods have approximately the same effective resolution. The solution of the wave propagation method is diffusive compared to the 3rd order RKDG and the 2nd order RKDG is even more diffusive. All values normalized to the initial peak values. Lower plots have an expanded scale to show the details of the solution.
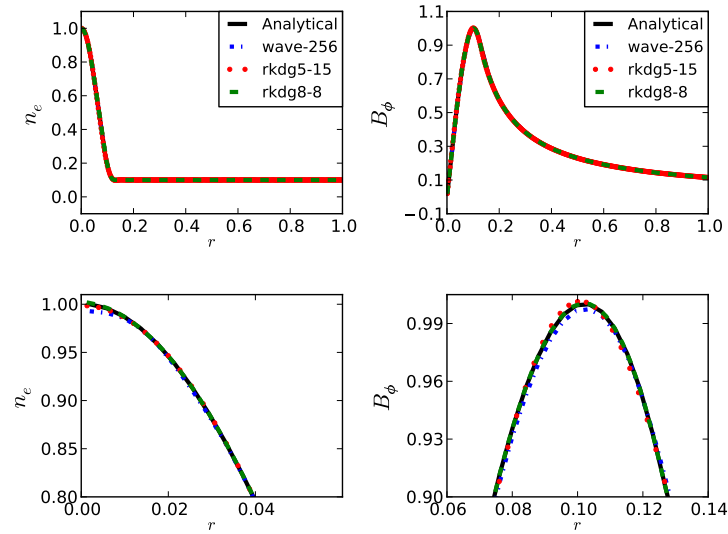
Figure 20: Electron number density and azimuthal magnetic field as functions of radius after 50 characteristic transit times are shown for the two-fluid axisymmetric Z-pinch equilibrium. The wave propagation method uses 256 cells, RKDG 5th order uses 15 cells and RKDG 8th order uses 8 cells so the effective resolutions of the RKDG solutions are about 1/3 and 1/4 that of the wave propagation solution. The low resolution, high spatial order RKDG solution holds equilibrium better than the wave propagation at 256 cells. All values normalized to the initial peak values. Lower plots have an expanded scale to show the details of the solution.

method, as seen in Table 7. The computational time required to advance the solution for 50 characteristic transit times for each method is also presented in Table 7. Each method has different CFL stability limit as shown in the 4th column of Table 7 based on Table 2.2 in [6] where the spatial and temporal orders are taken into account to determine the maximum CFL value.

Table 7: l_2-norm of electron number density to quantify accuracy for each method, and computational time required to advance the solution to 50 characteristic transit times to quantify computational effort for the two-fluid 1-dimensional Z-pinch.

Method	l_2-norm	Computational time to $t = 50$	CFL
WAVE_128	7.8×10^{-3}	3.7	1.0
WAVE_256	1.5×10^{-3}	13.8	1.0
RKDG2_64	1.3×10^{-2}	3.8	0.33
RKDG3_40	4.4×10^{-4}	5.4	0.21
RKDG5_15	1.7×10^{-3}	6.7	0.089
RKDG8_8	1.9×10^{-3}	5.7	0.04

The full two-fluid plasma model has imaginary eigenvalues for the source terms. Performing a source splitting for the wave propagation method causes the equilibrium decay. Bale et al. [5] discuss this problem and the treatment of the source terms. They deter-

mine that the source term handling through the process of splitting that has been applied to the wave propagation method might not work well for solutions close to steady-state. At equilibrium, the variation in fluxes must balance the source terms exactly and using split methods when the fluxes and sources are significant can introduce errors in the solution. Bale et al. suggest an alternate solution which involves only splitting the deviation from steady-state into waves. This is done by a process of distribution of the eigendecomposition of the source terms into the neighboring cells based on the sign of the corresponding eigenvalues. This, however, is not applicable to the case of the two-fluid plasma model. The source Jacobian for this equation system has all imaginary eigenvalues, so this unsplit method is not suitable here.

7.5 Axisymmetric Z-pinch equilibrium in 2-dimensions

A two-dimensional Z-pinch problem is investigated using the two-fluid plasma model. A perturbation is specified and evolved in time to see the resulting evolution of a two-fluid drift turbulence instability. The wave propagation and RKDG methods are compared for their abilities to capture the physics appropriately. The computational expense is also compared for the two methods.

The axisymmetric Z-pinch simulations use the same initial conditions and perturbations as in [27].

$$J_{zi} = 0, \tag{7.2a}$$

$$J_{ze} = \begin{cases} J_0, & \text{if } r < R_p, \\ 0, & \text{otherwise}, \end{cases} \tag{7.2b}$$

$$B_\phi = \begin{cases} \frac{1}{2} r \mu_0 J_0 [1 + \epsilon \sin(2\pi kz)], & \text{if } r < R_p, \\ \frac{1}{2} \frac{R_p^2}{r} \mu_0 J_0 [1 + \epsilon \sin(2\pi kz)], & \text{otherwise}, \end{cases} \tag{7.2c}$$

$$p = \begin{cases} p_0 - \frac{1}{4} \mu_0 J_0^2 r^2, & \text{if } r < R_p, \\ \alpha \mu_0 J_0^2 R_p^2, & \text{otherwise}, \end{cases} \tag{7.2d}$$

where R_p is the pinch radius, $p_0 = (1 + \alpha) \mu_0 J_0^2 R_p^2 / 4$, $\rho_i = (m_i / m_e) \rho_e = p / p_0$ and $p_i = p_e = p/2$. In these simulations, $R_p = 1/4$, $\alpha = 1/10$, $J_0 = 1$, $\epsilon = 1/100$ and k denotes the wave number. The ion-to-electron mass ratio is 25. In two-dimensions, the initial ion density profile is shown in Fig. 21.

Axis boundary conditions are implemented on the left edge and conducting wall boundary conditions are implemented on the right edge, just like the one-dimensional case. For the RKDG method, the axis and conducting wall boundary conditions are treated in the manner described in Section 7.1. Periodic boundary conditions are implemented on the top and bottom edges.

Due to the presence of large numerical dispersion in this problem, Lax-Friedrich fluxes are used with the RKDG method instead of Roe fluxes that are used for the wave propagation method.
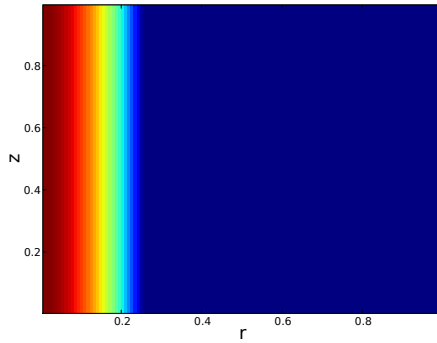
Figure 21: Initial conditions for ion density for a two-fluid Z-pinch equilibrium in 2-dimensions.
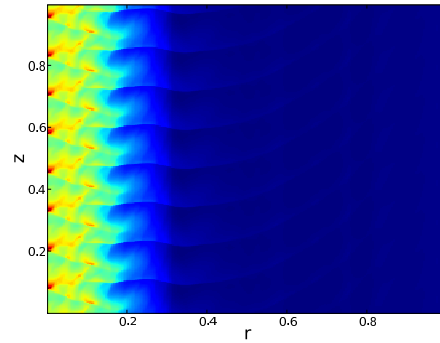

Figure 22: Ion density after 2 Alfven transit times for the two-fluid axisymmetric Z-pinch in 2-dimensions using the wave propagation method with a grid resolution of 1000×1000 cells. This high resolution solution is used as a benchmark.
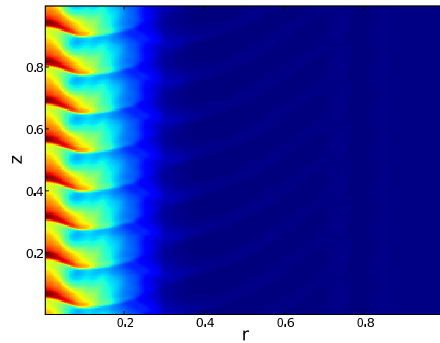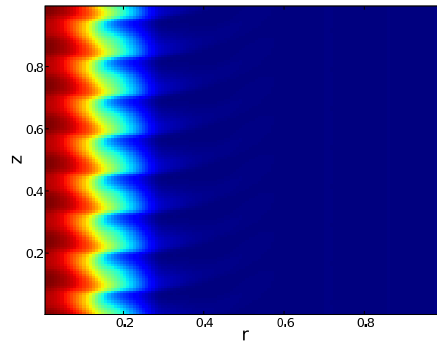

Figure 23: Ion density after 2 Alfven transit times for the two-fluid axisymmetric Z-pinch in 2-dimensions using the wave propagation method with a grid resolution of 128×128 (left plot) and 256×256 (right plot).

A sinusoidal perturbation as shown in Eq. (7.2c) with $k=8$ is applied to the azimuthal magnetic field, B_ϕ. The solution is then allowed to evolve for the wave propagation method with resolutions of 128×128 and 256×256 as shown in Fig. 23. This is compared to a 2nd order RKDG solution with resolutions of 64×64 and 128×128 and a 3rd order RKDG solution with a resolution of 128×128 as shown in Fig. 24. The plots shown are after 2 Alfven transit times.

The drift parameter for this system is $v_e/v_{si} \approx 8$, where v_e is the electron drift velocity and v_{si} is the ion sound speed. The ratio of the pinch radius to the ion Larmor radius, r_p/r_{Li}, is approximately 3. A high resolution solution using a 1000×1000 cell wave propagation method is shown in Fig. 22 as a benchmark for the wave propagation and RKDG solutions. This solution is compared to a 2nd order RKDG solution using 500×500 cells and it is verified that both methods converge to the same solution. Comparing Figs. 23 and 24 it is seen that both the wave propagation method and the RKDG
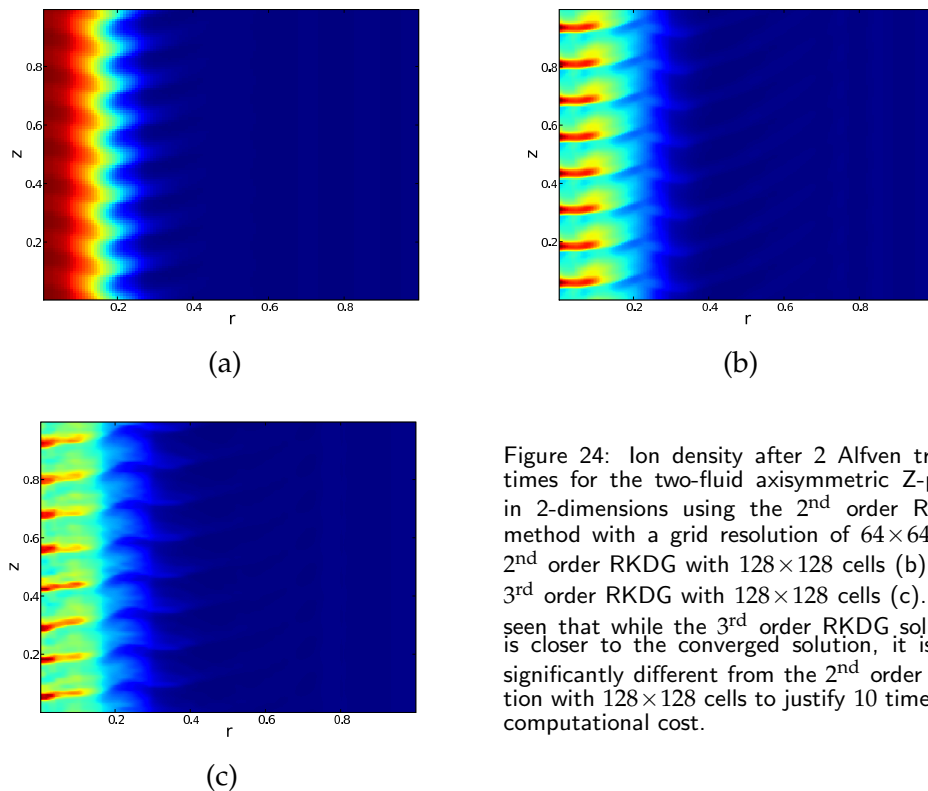
(a)

(b)

(c)

Figure 24: Ion density after 2 Alfven transit times for the two-fluid axisymmetric Z-pinch in 2-dimensions using the 2nd order RKDG method with a grid resolution of 64×64 (a), 2nd order RKDG with 128×128 cells (b), and 3rd order RKDG with 128×128 cells (c). It is seen that while the 3rd order RKDG solution is closer to the converged solution, it is not significantly different from the 2nd order solution with 128×128 cells to justify 10 times the computational cost.

method (at 2nd and 3rd order) capture 8 wavelengths of the short-wavelength instability. This is better seen from the instability growth rates of Fig. 25 where the perturbation in
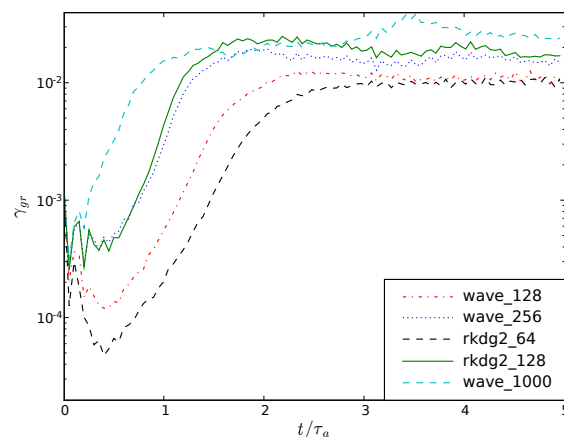

Figure 25: Growth rates for the perturbation in the magnetic field as a function of the time, t/τ_a, where τ_a is the Alfven transit time. It is observed that increasing the resolution makes the instability growth rates approach that of the high resolution solution.

magnetic field is measured against an unperturbed solution [27]. The growth rate of the instability is computed using

$$\gamma_{gr} = \iint |\Delta\mathbf{B}| 2\pi r dr dz, \tag{7.3}$$

where $\Delta\mathbf{B}$ refers to the difference in magnetic field between the solutions of a perturbed equilibrium and an unperturbed equilibrium. The unperturbed equilibrium solution is needed to account for oscillations that occur in the system since the equilibrium is not a true two-fluid equilibrium initially.

A five stage 4th order SSPRK time integration scheme [21] for the 2nd spatial order DG solution with 128×128 cells gives the same result as the middle plot in Fig. 24. Even though the SSP methods allow larger time steps, the physics of the two-fluid system, specially in highly nonlinear instability problems, like the Z-pinch, does not benefit from the increased accuracy. In fact a 2nd order TVB method gives almost exactly the same result as a 4th order SSP method. The presence of a large number of shocks in this problem requires limiting which reduces the accuracy of the overall solution. As a result, there appears to be no significant benefit in going to higher temporal orders in terms of computational effort or solution characteristics.

Fig. 25 shows that increasing the resolution causes the instability to set in sooner in time and have a greater slope. An increase in the resolution shows convergence towards the high resolution solution. The growth rates show that the 64×64 cell RKDG solution has the largest variation from the high resolution solution, while the 128×128 cell RKDG solution has the least. The instability is least to best resolved in the following order - 64×64 cell 2nd order RKDG solution, 128×128 cell wave propagation solution, 256×256 cell wave propagation solution, 128×128 cell 2nd order RKDG solution, 128×128 cell 3rd order RKDG solution. For the same effective resolution of 256×256, the 2nd order RKDG method takes about 1.3 times the computational effort of the wave propagation method. The wave propagation solution at a resolution of 256×256 takes about 9 times the computational effort of the 128×128 cell wave propagation solution. The 2nd order RKDG solution at a resolution of 128×128 takes about 7 times the computational effort of the 64×64 cell RKDG solution. At the same effective resolution of 256×256, the growth rates of the RKDG and wave propagation solutions are comparable. The short wavelength instability is better resolved at higher grid resolutions.

Comparing the 2nd and 3rd order RKDG solutions at a resolution of 128×128 in Fig. 24, it is seen that while the 3rd order solution is closer to the converged solution, using the 3rd order method instead of the 2nd order method may not be justified when taking the computational cost into account. The 3rd order solution uses the high-order limiters from [23]. The computational effort of the 3rd order solution is about 10 times that of the 2nd order solution for this resolution. The high-order limiters do not add significant computational cost as compared to the simple TVB minmod limiters. Most of the computational cost comes from solutions of the Riemann problem for each expansion coefficient at each cell interface, where the number of expansion coefficients for each conserved variable in-

creases substantially when the spatial order is increased. Doubling the grid resolution while using 2nd order for the RKDG method provides a more converged solution and only uses about 7 times greater computational effort. There might not be an advantage of going to higher-order RKDG solutions for this problem because the application of limiters locally reduces the solution to 1st order when sharp gradients are present. The solutions clearly have sharp gradients throughout the domain.

8   Conclusions

The wave propagation method and the Runge-Kutta Discontinuous Galerkin (RKDG) method are explored for equation systems with dispersive source terms. When the wave propagation method is run with a Courant number of 1 for equation systems that only have one characteristic speed of disturbance propagation, the solution obtained is close to the analytical or converged solution without significant dispersive or diffusive errors.

For the ion cyclotron waves in the dispersive Euler equation system, the presence of dispersive source terms causes phase errors when using the wave propagation method with large source terms. This results when a characteristic frequency is high compared to the frequency of information propagation. These errors occur due to the source term splitting employed in the wave propagation method. The RKDG method is not a split method and therefore does not produce such phase errors. Even using a low resolution grid and a high spatial order, the RKDG method provides an accurate solution for dispersive equations. Using higher grid resolutions for the wave propagation method eliminates these phase errors; however, it is more computationally expensive than a lower-resolution, higher-order RKDG solution which provides a comparable solution. In plasma physics, it is important to study equation systems that have source terms with imaginary eigenvalues such as the dispersive Euler equations and the two-fluid plasma model where the dispersive effects of the source terms need to be handled accurately to capture the physics correctly.

The two-fluid plasma model is explored for a one-dimensional soliton propagation, an axisymmetric one-dimensional pulse problem and a one- and two-dimensional Z-pinch equilibrium. For the soliton propagation, it is observed that the RKDG method with higher order is more computationally efficient than the wave propagation method which is subject to phase errors in the propagating pulses similar to the ion cyclotron waves in the dispersive Euler equation system. For the one-dimensional two-fluid pulse problem, it is seen that the RKDG method performs better than the wave propagation method when computational effort and convergence are taken into account. The solution using the wave propagation method is more diffusive for the fluid variables. This is due to the disparate characteristic speeds in the two-fluid plasma model, namely the fluid speeds of sound and the speed of light. The wave propagation method is run using a maximum Courant number of 1 for one-dimensional problems. The time step is calculated based on the fastest characteristic speed in the system as a result of which

the information propagating at slower speeds can be diffused away. This is not the case for the RKDG method because it uses higher spatial and temporal orders of accuracy to provide more accurate solutions. For the one-dimensional Z-pinch problem, the RKDG method holds equilibrium better than the wave propagation method. This is attributed to the source term splitting in the wave propagation method as discussed previously. This is a problem with equilibrium applications of the wave propagation method and has been studied by Bale et al. [5] Unsplit methods are not applicable to the two-fluid plasma model because the source Jacobian in this equation system has imaginary eigenvalues. For the same computational expense, RKDG holds equilibrium better even when using a lower resolution with higher order as compared to the wave propagation method with higher resolution.

It is important to study dynamic solutions such as a two-fluid Z-pinch problem in two-dimensions with a small initial perturbation applied to the equilibrium. It is seen that both the wave propagation and the RKDG methods are able to capture the small-scale two-fluid drift turbulence instability. Increasing the grid resolution causes the instability growth rates to approach that of the converged solution. The RKDG method takes 1.3 times more computational effort to provide a solution for the same effective grid resolution as compared to the wave propagation method. Comparing the 2$^{\text{nd}}$ order RKDG method and the wave propagation method at the same effective grid resolution of 256×256, the growth rates are comparable. Whereas, at a lower effective resolution of 128×128 cells, the wave propagation better captures the instability as compared to the 2$^{\text{nd}}$ order RKDG method with 64×64 cells. Using higher orders for the RKDG solution does not seem to be advantageous for this problem as the limiters reduce regions of sharp gradients to first order accuracy even when high-order limiters are used. When using the RKDG method for problems with shocks, increasing the grid resolution while using 2$^{\text{nd}}$ spatial order provides a more converged solution and uses less computational effort than increasing the spatial order.

Acknowledgments

References

[1] A. G. Kulikoviskii, N. V. Pogorelov, and A. Y. Semenov, Mathematical Aspects of Numerical Solutions of Hyperbolic Systems, Chapman and Hall/CRC, 2001.

[2] R. J. LeVeque, Finite Volume Methods for Hyperbolic Problems, Cambridge University Press, 2002.

[3] A. Hakim, Extended MHD modelling with the ten-moment equations, J. Fusion. Energy., 27 (2008), 36–43.

[4] A. Hakim, J. Loverich, and U. Shumlak, A high resolution wave propagation scheme for ideal two-fluid plasma equations, J. Comput. Phys., 219 (2006), 418–442.

[5] D. Bale, R. J. LeVeque, S. Mitran, and J. A. Rossmanith, A wave-propagation method for conservation laws and balance laws with spatially varying flux functions, SIAM J. Sci. Comput., 24 (2002), 955–978.

[6] B. Cockburn, and C.-W. Shu, Runge-Kutta discontinous Galerkin methods for convection-dominated problems, J. Sci. Comput., 16 (2001), 173–261.

[7] B. Cockburn, G. E. Karniadakis, and C.-W. Shu, The Development of Discontinuous Galerkin Methods, in: Discontinuous Galerkin Methods: Theory, Computation and Applications, Lecture notes in Computational Science and Engineering, Volume 11, Springer, 2000.

[8] W. H. Reed, and T. R. Hill, Triangular mesh methods for the neutron transport equation, Technical Report LA-UR-73-479, Los Alamos Scientific Laboratory, 1973.

[9] B. Cockburn, and C.-W. Shu, TVB runge-Kutta local projection discontinous Galerkin finite element for conservation laws II-general framework, Math. Comput., 52(186) (1989), 411–435.

[10] C.-W. Shu, Total-variation-diminishing time discretizations, SIAM J. Sci. Stat. Comput., 9(6) (1988), 1073–1084.

[11] F. Bassi, and S. Rebay, A high order accurate discontinuous finite element method for the numerical solution of the compressible Navier-Stokes equations, J. Comput. Phys., 131 (1997), 267–279.

[12] J. T. Oden, I. Babuŝka, and C. E. Baumann, A discontinuous *hp* finite element method for diffusion problems, J. Comput. Phys., 146 (1998), 491–519.

[13] B. Cockburn, F. Li, and C.-W. Shu, Locally divergence-free discontinuous Galerkin methods for the Maxwell equations, J. Comput. Phys., 194(2) (2004), 588–610.

[14] J. S. Hesthaven, and T. Warburton, High-order nodal discontinuous Galerkin methods for the Maxwell eigenvalue problem, Royal. Soc. London., 362 (2004), 493–524.

[15] F. Li, and C.-W. Shu, Locally divergence-free discontinuous Galerkin methods for MHD equations, J. Sci. Comput., 22-23 (2003), 413–442.

[16] D. Levy, C.-W. Shu, and J. Yan, Local discontinuous Galerkin methods for nonlinear dispersive equations, J. Comput. Phys., 196 (2004), 751–772.

[17] M. Zhang, and C.-W. Shu, An analysis of and a comparison between the discontinuous galerkin and the spectral finite volume methods, Comput. Fluids., 34 (2005), 581–592.

[18] J. Loverich, and U. Shumlak, A discontinuous Galerkin method for the full two-fluid plasma model, Comput. Phys. Commun., 169 (2005), 251–255.

[19] U. Shumlak, and J. Loverich, Approximate Riemann solver for the two-fluid plasma model, J. Comput. Phys., 187 (2003), 620–638.

[20] R. J. Spiteri, and S. J. Ruuth, A new class of optimal high-order strong-stability-preserving time discretization methods, SIAM J. Numer. Anal., 40(2) (2002), 469–491.

[21] S. Gottlieb, D. I. Ketcheson, and C-W. Shu, High order strong stability preserving time discretizations, J. Sci. Comput., 38(3) (2008), 251–289.

[22] B. Cockburn, S. Hou, and C.-W. Shu, The Runge-Kutta local projection discontinuous Galerkin finite element method for conservation laws iv: the multidimensional case, Math. Comput., 54 (1990), 545–581.

[23] Lilia Krivodonova, Limiters for high-order discontinuous Galerkin methods, J. Comput. Phys., 226 (2007), 879–896.
[24] J. Qiu, and C.-W. Shu, Runge-Kutta discontinuous Galerkin method using WENO limiters, SIAM J. Sci. Comput., 26 (2005), 907–929.
[25] C. D. Munz et al., Divergence correction techniques for Maxwell solvers based on a hyperbolic model, J. Comput. Phys., 161 (2000), 484–511.
[26] S. Baboolal, Finite-difference modeling of solitons induced by a density hump in a plasma multi-fluid, Math. Comput. Sim., 55 (2001), 309–316.
[27] J. Loverich, and U. Shumlak, Nonlinear full two-fluid study of $m=0$ sausage instabilities in an axisymmetric Z-pinch, Phys. Plasmas., 13 (2006), 082310.